Talanta 94 (2012) 9–21

Contents lists available at SciVerse ScienceDirect

Talanta

journal homepage: www.elsevier.com/locate/talanta

On the chemical identification and determination of flavonoids in solid-state

Bojidarka B. Ivanova*, Michael Spiteller

Institute of Environmental Research, University of Dortmund, Otto–Hahn-Strasse 6, 44221 Dortmund, Germany

ARTICLE INFO

Article history:
Received 27 September 2011
Received in revised form 2 December 2011
Accepted 6 December 2011
Available online 9 December 2011

Keywords:
Forensic chemistry
Solid-state mixtures
Raman spectroscopy
MALDI-mass spectrometry
Natural products
Alkaloids

ABSTRACT

The paper presented with qualitative and quantitative analysis of alkaloids in solid-state, using the excitations within the THz-spectroscopic region of 300–30 cm^{-1} (9.00–0.9 THz). Series of nine plant flavonoids (FLs) and their mixtures were analyzed both qualitatively and quantitatively. For first time in the literature was reported the quantitative analysis of alkaloids and their mixtures within the THz-region using the solid-state Raman spectroscopy, and matrix-assisted laser desorption/ionization (MALDI) mass spectrometry (MS). The calibration and validation, concentration limit of detection (*LOD*), limit of quantification (*LOQ*), and linearity limit (*LL*) were obtained. The chemometric nonlinear and linear approaches for analysis and interpretation of the quantities were applied. The results obtained were compared with a parallel *QA*, using the calibrated and validated HPLC electrospray ionization (ESI) mass spectrometric method, electronic absorption (EAs) and CD spectroscopy. The metrology, including accuracy, measurement repeatability (intra-serial precision condition of measurement), measurement precision, trueness of the measurement, and reproducibility of the measurement, measurement bias and errors of the measurements were discussed.

1. Introduction

The recent developments on the qualitative and quantitative analysis (*QA*) of small molecules by THz-spectroscopy [1d,e] for the needs of the forensic science have been shown successful results on the identification of many explosives, chemical and biological agents [1,2]. The *QA* of the solid-binary mixtures has been shown the concentration *LOD* ± 5% of the analyzing of the macro component [1e]. Recent analytical studies of the excitation phenomena of pharmaceutics within the same region, by the solid-state Raman spectroscopy [3] have been provided data for concentration *LOD* of 1.34% of the analyte, using the nonlinear chemometric approaches [3i,j]. It has been shown as well that the complementary application of the vibrational spectroscopy and MALDI method expand the capability for analysis of multicomponent mixtures within concentration range 10^{-5} to 10^{-7} mol/l [3j]. The individual spectroscopic profiles in the vibrational spectra of molecules in solid-state, observed within the THz-region and the high intensity of the observed excitations, expand the applicability of the method for *QA* of the properties of the evidences that could be attributed to a common source with an extremely high degree of certainty [2e–h]. In this respect, the development of the method for the needs the forensic chemistry, lie in the systematic investigations of the different classes of natural products (NPs), semi- and synthetic analogous, updating the databases, and optimizing the software allowing quickly, conveniently and accurately usage of the method for obtaining of the pertinent investigative information [2]. Thus, the paper reported a complementary analytical application of solid-state Raman spectroscopic and mass spectrometric study of nine flavonoids (Scheme 1) as well as their mixtures. The validation of the methods, metrology including, accuracy, precision, measurement repeatability, trueness of the measurements, reproducibility of the measurement, measurement bias and errors of the measurements, concentration *LOD* and *LOQs*, as well as *LL* were discussed.

2. Experimental

2.1. Materials

The FLs were obtained according [3]. The synthesis of *bis*(R-(+)-1-phenylethylammonium) squarate **Sd**-(**1**), was obtained by mixing of squaric acid (Sigma) and R-(+)-1-phenylethylamine at molar ratio 2:1 in 20 ml solvent mixture methanol:water 1:1 under stirring for 30 min at 150 °C. The resulting colorless crystals, were filtered off, washed with CH_3OH and dried on P_2O_5 at 298 K. The data from the performed elemental analisys were: found: C, 67.40; H, 6.76; N, 7.88; calcd. for $C_{20}H_{24}O_4N_2$: C, 67.38; H, 6.79; N, 7.86%, yield 91%, respectively.

* Corresponding author. Tel.: +49 231 755 4089; fax: +49 231 755 4085.
E-mail address: B.Ivanova@infu.tu-dortmund.de (B.B. Ivanova).

0039-9140/$ – see front matter © 2011 Elsevier B.V. All rights reserved.
doi:10.1016/j.talanta.2011.12.016

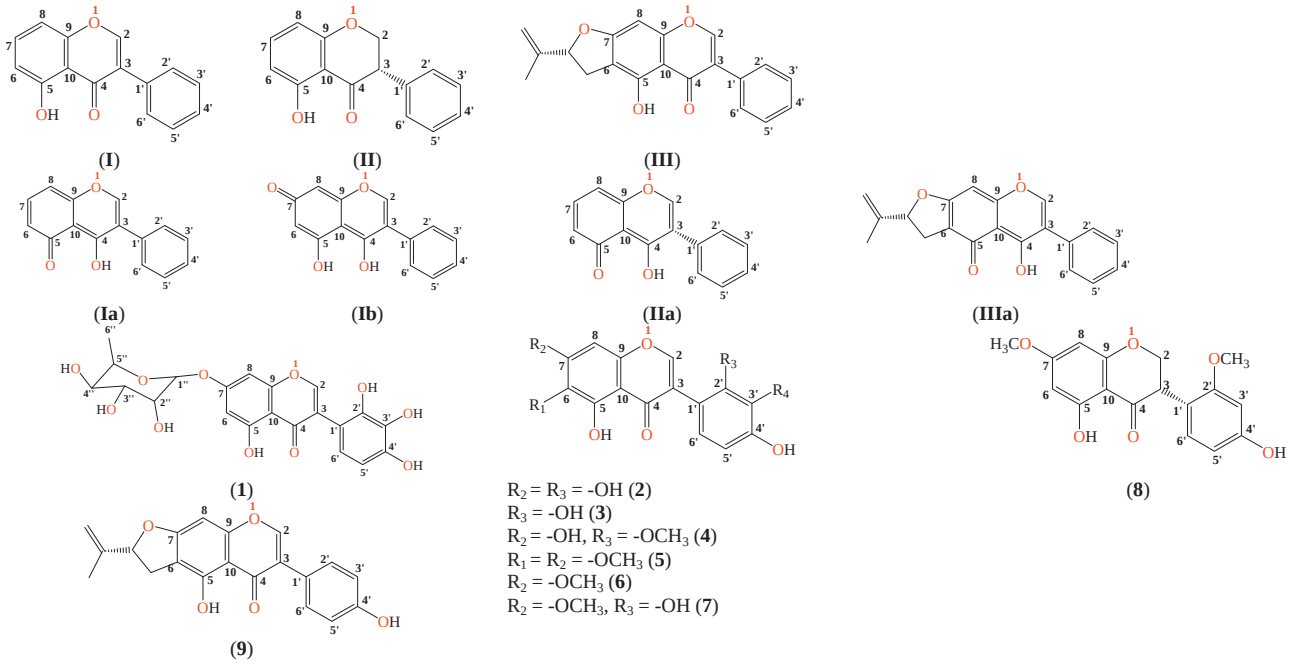

Scheme 1. Chemical diagrams of FLs (1)–(9); common molecular skeleta (I–III), the resonance (Ia,b, IIa, IIIa) forms, depending of the pH.

2.2. Physical methods

The X-ray diffraction intensities were measured on a Bruker Smart X2S (Bruker AXS, Karlsruhe, Germany) diffractometer, using micro source Mo-K_α radiation and employing the ω scan mode. The data were corrected for Lorentz and polarization effects. An absorption correction procedure, based on multiple scanned reflections was applied. The Sd-(1) structure was solved by direct methods using SHELXS-97 [4] and was refined by full-matrix least-squares refinement against F^2 [4]. Anisotropic displacement parameters were introduced for all non-hydrogen atoms. The hydrogen atoms attached to carbon were placed at calculated positions and refined allowing them to ride on the parent carbon atom. The hydrogen atoms bound to nitrogen and the oxygen were constrained to the positions which were confirmed from the difference map and refined with the appropriate riding model. The experimental data were summarized in Table S1. The spectra were recorded at ambient conditions (T = 298 K, P = 1 atm). The powder X-ray diffraction measurements were carried out on polycrystalline samples, proving the crystallographically obtained space systems. The XRD patterns were obtained using a Rigaku MiniFlex powder diffraction system (Rigaku Corp., Osaka, Japan), equipped with a horizontal goniometer in the $\theta/2\theta$ mode. The X-ray source was nickel-filtered K-α emission of copper (1.54056 Å). Samples were packed into an aluminum holder using a back-fill procedure and will be scanned over the range of 50–6° 2θ, at a scan rate of 0.5° 2θ/min. Using a data acquisition rate of 1 point per second, the scanning parameters equate to a step size of 0.0084° 2θ. Calibration of each powder pattern will be effected using the characteristic scattering peaks of aluminum at 44.738 and 38.472° 2θ. The method was applied for elucidation of the crystallographic space system of the matrixes during the same preparation technique for MALDI measurements.

HPLC–MS/MS measurements were made using TSQ 7000 instrument (Thermo Fisher Inc., Rockville, MD, USA). Two mobile phase compositions were used: (A) 0.1% (v/v) aqueous HCOOH and (B) 0.1% (v/v) HCOOH in CH_3CN. Electrospray ionization mass spectrometry. A triple quadrupole mass spectrometer (TSQ 7000 Thermo Electron, Dreieich, Germany) equipped with an ESI 2 source was used and operated at the following conditions: capillary temperature 180 °C; sheath gas 60 psi, corona 4.5 μA and spray voltage 4.5 kV. Sample was dissolved in acetonitrile (1 mg ml^{-1}) and was injected in the ion source by an autosampler (Surveyor) with a flow of pure acetonitrile (0.2 ml/min). Data processing was performed by Excalibur 1.4 software. A standard LTQ Orbitrap XL (Thermo Fisher Inc.) instrument was used for the MALDI-MS measurements, using the UV laser source at 337 nm. An overall mass range of m/z 100–1000 was scanned simultaneously in the Orbitrap analyzer. The ImageQuest 1.0.1 program package was used. The laser energy values were within 12.5–17.2 μJ. The numbers of averaged laser shots lies within 16–108, the MALDI flow rate values were within 24.8–27.2; the acquisition time was within 30.2–137.2 min, the corresponding elapsed scan time range lies within 20.2–3.77 s, respectively.

Raman spectra in solid-state were recorded on: (i) Nicolet NXR 9610 FT-Raman spectrometer (both instruments were products of Thermo Electron Corporation, Baltimore, MD, USA), equipped with the semiconductor laser operating source at 976 nm. The resolution of 0.09 cm^{-1} was over the spectral range 100–3705 cm^{-1} and (ii) Horiba Jobin–Yvon Inc. (Edison, NJ, USA) 60000 triple monochromator spectrometer equipped with a Spectra-Physics Inc. (Mountain View, CA, USA) model 164 argon ion laser operated on the 514.5 nm line. The resolution of 1.0 cm^{-1} was over the spectral range 20–2500 cm^{-1}. A triple integrated laser system was used for the variation of the excitation energy at 532, 633 and 785 nm, respectively. The laser power used was 100 mW, with a spectral band-space of 3 cm^{-1}. The spectra were recorded at ambient conditions (T = 298 K, P = 1 atm). The Raman spectra of the solid crystal powders were measured in a glass capillary.

Chromatographic confirmation about the purity of the studied compounds was performed with a Gynkotek (Germering, Germany) HPLC instrument, equipped with a preparative Kromasil 100 C18 column (250 mm × 20 mm, 7 μm; Eka Chemicals, Bohus, Sweden) and a UV detector set at 250 nm. The mobile phase was acetonitrile:water (90:10, v/v) at a flow rate of 4 ml/min. The analytical HPLC was performed on a Phenomenex (Torrance, CA, USA) RP-18 column (Jupiter 300, 150 mm × 2 mm, 3 μm) under the same chromatographic conditions as above. The QA was performed on a Shimadzu UFLC XR (Kyoto, Japan) instrument, equipped with

an auto sampler, PDA, an on-line degasser and column thermostat. As stationary phase a Phenomenex Luna Phenyl-Hexyl column (150 mm × 3 mm i.d., 3 μm particle size) was used. The mobile phase consisted of 0.02% (v/v) TFA in water (solvent A) and acetonitrilemethanol 75:25 (v/v; solvent B). Separation was achieved by a gradient analysis starting with 55A–45B, increasing the amount of solvent B in 30 min to 75% and 30.1 min to 100% B, stop time 40 min. For equilibration a post time of 15 min was applied. Other parameters: flow rate 0.30 ml/min, injection volume 5 μl, detection wavelength 280 nm; column temperature 35 °C.

2.3. Computational methods

2.3.1. Statistical and mathematical approaches (chemometrics)

The experimental and theoretical spectroscopic patterns were processed by R4Cal OpenOffice STATISTICs for Windows 7 [5] program package. Baseline corrections and curve-fitting procedures were applied. Details were shown in corresponding supporting information file. The curve-fitting nonlinear procedure was applied for the data interpretation. In the case of the Levenberg–Marquardt method, the merit equation used is χ^2 the equation. The final solution is found when a minimum in the reduced χ^2 equation is reached. It is a statistical measure of "goodness-of-fit", inversely proportional to the known variance of the data set. The statistical significance of each regression coefficient was checked by the use of *t*-test. The model fit was determined by *F*-test [5]. The statistical multiple linear regression (MLR) analysis and AVOVA test were also used for chemometric evaluation of the obtained quantities [5,3i,j].

The test of the statistical significance was performed evaluating the *p*-values, representing the probability of the obtained statistics at least as extreme as the one that was actually observed. The test consists of the assumption that the null hypothesis is true. Rejecting the last hypothesis, is when the *p*-value is less than the 0.05 or 0.1, or for the obtained data set is statistically significant.

A *t*-test is statistical hypothesis test in which the Student's *t*-distribution is followed, if the null hypothesis is supported. Similar to the *t*-test, *F*-test is any statistical test, where in which the statistic has an *F*-distribution at the null hypothesis. Exact *F*-tests is applied when the data sets have been fitted by least squares.

Details of the performed multiple linear regression (MLR) and Analysis of variance (ANOVA) for MLR, would find in [3i].

2.3.2. Quantum chemical approaches

Quantum chemical calculations were performed with Gaussian 09 and Dalton 2.0 program packages [6]. The geometries of the studied species were optimized at two levels of theory: second-order Moller–Pleset perturbation theory (MP2) and density functional theory (DFT) using the 6-31++G(d,p) basis set. The DFT method employed was B3LYP, CAM-B3LYP, and M06-2X functionals. Molecular geometries of the studied species were fully optimized by the force gradient method using Bernys' algorithm. For every structure the stationary points found on the molecule potential energy hypersurfaces were characterized using standard analytical harmonic vibrational analysis. The absence of the imaginary frequencies, as well as of negative eigenvalues of the second-derivative matrix, confirmed that the stationary points correspond to minima of the potential energy hypersurfaces. The calculation of vibrational frequencies and infrared intensities were checked to establish which kind of performed calculations agree best with the experimental data. The electronic spectra in gas phase and solution were obtained, by time-dependent density functional method (TD-DFT) method. The 6-311++G(2d,p) and large "correlation consistent" basis sets aug-cc-pVDZ and aug-cc-pVTZ were used. To describe the species in aqueous solution we use both an explicit supermolecule and microhydration approach, in which several water molecules were coordinated to the solute at the optimized geometry of the supermolecule, and a polarizable continuum approach (PCM). The protonation ability of the studied model systems was elucidated by the natural bond orbital (NBO) charges and analysis [6].

2.4. Quantitative analysis procedure

2.4.1. Validation of the Raman method

For the purpose of the quantitative determination were attributed the integral intensities defined as $A\nu_i^{(j,k)}$ at the ν_i frequency for the *j*- and *k*-components, common for both the analyzed substances in the mixtures to the corresponding value $A\nu_i^{(j)}$ for a frequency presented in the corresponding solid-state Raman spectra [3i,j,5s–w].The $A\nu_i^{(j)}$ measured in the Raman spectrum depends on the intensity of the laser I_o, on a factor $K(\nu_i)$ including the frequency dependent terms (such as overall spectrophotometer response, self-absorption of the medium and molecular scattering of the Raman active species), and on the mole fraction (X) of the active species. For the two component mixtures, the corresponding equations were shown in [3i,j].

A calibration curves relating the Raman intensity to concentration and the validation of the HPLC–MS/MS data were prepared and evaluated. The Raman signals were too weak to detect, even the most intense frequencies when the concentration *LOD* of the quantified component in a binary systems was less than 1.30%. The corresponding *LOQ* value was 4.333%. This was attributed to a critical concentration. There was evidence of saturation of the signals at higher concentrations above 12:1 of the analyzed component. The fitting procedure, using the quadratic and linear logarithmic dependence resulted to the r^2 values of 0.88325 and 0.97652. Thus, examination of the variation of the band intensities in the full range of concentrations was performed within shown concentration interval, confirming the linear dependences, thus defining the linearity limit (*LL*) of the intensity of the signals versus the concentration. The obtained results were discussed in the text.

The concentration limit of detection (*LOD*) and the limit of quantification (*LOQ*) were determined according to the equations [3o]:

$LOD = 3S_b/a$ and $LOQ = 10S_b/a$, where S_b is the standard deviation of the intercept and a is the slope.

2.4.2. Quantification and validation of the HPLC-ESI–MS/MS method

The calibration and quantitative analysis by the HPLC-ESI–MS/MS was performed using the parameters: r^2, specifying the threshold for the *goodness of fit* of the calibration curve, calculating the coefficient of determination r^2 whenever it computes a calibration curve. If the value was less than the r^2 threshold, the data were set to *true*. A goodness of fit calculated for calibration curves, indicates that the calibration curve passes through each data point, when $r^2 = 1.0000$ (optimal value); Concentration *LOD* – If the quantified component concentration was less than the *LOD* threshold, the detection limit in the results was set to true; *LL* – the quentity allows to specify a threshold for the linearity limit; *LOQ* – it allows to evaluate the threshold for the limit of quantitation. If the quantified component concentration was less than the LOQ threshold, the quantitative limit in the results was set to *true*.

Nevertheless that the perfumed quantitative analysis was within the *LL*, both for the validation of the HPLC-ESI–MS/MS as well as the Raman spectroscopic dependences, where at the high concentration regions the deviation of the linearity of the obtained dependences of the intensity of the modes versus the concentration the following calibration curves were used and the data were evaluated statistically. For the cases where out of the *LL* was observed, a discussion was performed in the text: Quadratic curve – calibration curve in which were calculates a quadratic (second order) polynomial least-squares fitting by the mathematical form: $y = ax^2 + bx + c$,

where a, b, and c were polynomial coefficients; Linear dependence of the logarithmic functions – a linear polynomial least-squares fitting, the equation: $\ln[y] = a.\ \ln[x] + b$, where a was the slope of the curve and b was the intercept point on the y-axis; Quadratic logarithmic function: represent fitting, where a quadratic (second order) polynomial least-squares method was used, calculating the dependences according the equation: $\ln[y] = a\ \ln[x^2] + b\ \ln[x] + c$, where a, b, and c were the corresponding polynomial coefficients.

Avalon algorithms were applied for the peak detection. The component identification in the mass chromatograms of the multicomponent mixtures was consisted in the identification of the chromatographic peak mathematically, comparing the actual retention time (RT) of the peak to the expected RT for the component of interest. The last quantity was determined preliminary. The component identification in the mass spectra of the mixtures was performed, comparing the molecular ion and/or fragment ions of the component with the MS of a known compound. In addition depending of the specificity, the identification was obtained, comparing fragmentation product ions by MS/MS with the corresponding ions in the MS of a known compound.

2.5. Metrology

The *accuracy*, consisting of the closeness of agreement between the measured quantity and the true one was evaluated, using the obtained measurement errors. Since accuracy is not quantity and is not given as numerical value, the smaller measurement errors were an indication for the accurate results (Tables 1, 2 and 4).

The *trueness of measurement*, representing the closeness of agreement between the average quantity of the infinite number of replicate measurements and reference quantity was evaluated. Since, the measurement trueness is not a quantity and cannot be expressed numerically, as well as has not available ISO standards for the these flavonoids, in our study the trueness was evaluated, using the average quantity of three repeated measurements, comparing with the values obtained from the measurements of the standard (compound (2) prepared as standard, and Tables 4–6). The evaluation in the presented data, was performed taking into account that the measurement trueness is inversely related to systematic measurement error (SME), but is not related to random measurement error (RME, RME = ME–SME).

The *precision*, i.e. closeness of agreement between indications or measured quantity values obtained by replicate measurements on the same or similar objects under specified conditions, was evaluated by the repeated measurements of the same FLs under the same specified conditions (Tables 3–6). The measurement precision was expressed numerically by measures of imprecision, such as standard deviation (SD), variance, and/or coefficient of variation under the specified experimental conditions.

The measurement bias, estimating of a systematic measurement error, was evaluated for both the methods.

Since, a condition of measurement was accepted as a repeatability condition, only with respect to a specified set of repeatability conditions, the presented data on the *repeatability condition of measurement*, were evaluated out of a set of conditions that includes the same measurement procedure, same operators, same measuring system, same operating conditions and same location, and replicate measurements on the same in our case compounds of study over a short period of time (in our case consequently measurements).

The *reproducibility condition of measurement*, i.e. out of a set of conditions that includes different locations, operators, measuring systems, and replicate measurements on the same compounds, was evaluated by the obtained data from the different measuring systems, using both the same and modified measurement procedures for the HPLC-ESI–MS/MS.

2.6. Sample preparation techniques in solid-state for MALDI-MS analysis

All solvents used for isolation were purchased from VWR Int. (Darmstadt, Germany). Acetonitrile, methanol, and trifluoroacetic acid were of HPLC grade (Merck, Darmstadt, Germany). Ultrapure water was produced by a Sartorius Arium® 611 UV water purification system (Göttingen, Germany). As standard solvent for sample solutions, a mixture of methanol/water (1:1, v/v) was used (Uvasol®, Merck). The 2,5-dihydroxybenzoic acid (DHB, Merck) was used as matrix for MALDI measurements. As standard solvent for sample solutions, a mixture of methanol/water (1:1, v/v) was used. The dried droplet standard sample preparation technique was applied, using the 1 mol/l concentration of the matrix solution plus and analyte (FLs) solutions (10^{-4} to 10^{-7} M), both dissolved in methanol/water (1:1, v/v) solvent mixtures. The obtained solutions were mixed on the MALDI target and dried by a gentle flow of air. The same analyte solutions were used for ESI–MS measurements, using the acetonirile:methanol solvent mixtures 1:1 [4]. The corresponding MLR and ANOVA analysis of the MALDI MS data was performed. The integration was performed in the continuous term of the dependences of the relative and absolute abundance.

3. Results and discussion

3.1. Concentration limit of detection and quantification, linearity limit, validation, accuracy, measurement repeatability and precision, trueness of the measurement, reproducibility of the measurement, and assignment of the solid-state Raman spectra within THz-region

The Raman spectra of the FLs within the THz-region were elucidated qualitatively and quantitatively (Fig. 1). Similar the EAs and CD data, the spectroscopic patterns were interpreted by chemometric approaches (supporting information, [3i,j]). Similar to the spectra of drugs [3i,j] the H-bond deformations were observed within 200–110 cm^{-1} (6.0–3.0 THz), while the skeletal modes were found within 100–60 cm^{-1} (3.0–1.8 THz). The torsion of entire side chain vibrations about the aromatic system was assigned to 60 cm^{-1} (1.8 THz). The individual characteristic profile of the Raman spectra required an individual approach for *QA* of the FLs in mixtures, using common characteristic excitation versus the individual mode, characteristic for each of the compounds. It was important to note, that the minimal level overlapping effect, significant value of the signal-to-noise (S/N) ratio and relatively strong intensity of the signals were base requirements for *QA*, allowing to achieved the low concentration *LOD* [3i,j]. As shown in the spectrum of (2) in Fig. 1, the low S/N value within the 300–250 cm^{-1} region resulted to the confidence level of 98.00%, defining the quantity of the peaks at 296 and 233 cm^{-1} (Table 1). The data for $\nu_i^{(j)}$ and $A\nu_i^{(j)}$ for each of the studied systems were summarized in Table 1. The chemometric analysis was performed, using three consequently repeat measurements of the three sample preparations of each of the isolated compounds or mixtures (Table 2 and Fig. 2). The calculated p- and t-data were compared with tabulated data and indicated a 99.11% confidence level, to verify the absence of statistically significant differences. The accuracy, measurement repeatability and precision were evaluated by the data in Table 1. The spectroscopic data of mono- and multicomponent mixtures (Fig. 1 and Table 3) were procedure by the non-linear curve-fitting method, using the Lorenzian–Gaussian mixed functions at ratio 1:1 at 2000–4000 iterations, according our preliminary study on the quantitative determination of pharmaceutical produces [3i,j]. The obtained p-value of 0.0012 was indicated the statistical significance of the

Table 1
The obtained experimental data fom the solid-state Raman spectra of the FLs (1)–(9) accordimng the labelling Scheme 1.

(1)				(2)				(3)			
Area (A^j)	Center (ν^j)	Width	Height	Area (A^j)	Center (ν^j)	Width	Height	Area (A^j)	Center (ν^j)	Width	Height
25972 ± 2.29	389.27 ± 0.66	12.552	1650.9								
25972 ± 1.19	344.64 ± 0.54	15.676	1063.8								
83643 ± 3.28	309.87 ± 0.18	18.826	3545.0								
45426 ± 1.26	286.03 ± 0.93	12.755	2841.5	70671 ± 1.18	296.58 ± 0.13	24.290	2321.4				
88783 ± 3.19	273.90 ± 0.77	10.425	6795.1								
23481 ± 2.01	235.69 ± 0.93	21.540	6795.1	48029 ± 2.33	233.92 ± 0.23	33.648	1138.9				
				15689 ± 1.02	190.92 ± 0.44	9.7092	1289.3				
				20292 ± 0.33	176.53 ± 0.73	8.2505	1962.4	81086 ± 1.10	150.24 ± 0.10	18.127	3569.1
$1.9435.10^5$ ± 3.28	152.49 ± 0.03	348.24	869.79	55888 ± 0.89	152.43 ± 0.11	14.687	3036.2	75503 ± 2.01	142.59 ± 0.21	25.351	2376.3
12612 ± 2.55	130.38 ± 0.10	5.679	1771.7	$1.01.10^5$ ± 0.55	129.45 ± 0.33	13.682	5911.5	$4.6271.10^5$ ± 2.33	105.67 ± 0.17	18.641	19805
8589.2 ± 2.19	112.01 ± 0.22	6.018	1138.8	1.6010^5 ± 0.83	110.55 ± 0.77	14.255	8959.5	$1.2538.10^5$ ± 3.10	92.986 ± 0.23	5.8561	17083
				1.02310^5 ± 0.99	95.927 ± 0.79	8.5754	9526.1	$4.7814.10^5$ ± 1.25	83.664 ± 0.88	9.1845	41537
				1.6910^5 ± 0.83	83.815 ± 0.12	17.069	7930.0	$1.0030.10^5$ ± 5.10	71.086 ± 0.31	6.0114	13313
								64874 ± 3.19	60.505 ± 0.68	5.5265	9366.1
3451.2 ± 7.39	62.01 ± 0.52	2.231	831.7	70704 ± 0.66	64.610 ± 0.55	8.1251	6943.1	$1.7838.10^5$ ± 4.99	47.839 ± 0.22	7.0701	20130

(4)				(5)				(6)			
Area (A^j)	Center (ν^j)	Width	Height	Area (A^j)	Center (ν^j)	Width	Height	Area (A^j)	Center (ν^j)	Width	Height
				$1.2893.10^5$ ± 2.11	140.50 ± 0.02	56.744	1812.9	38156 ± 1.10	161.44 ± 0.10	8.4568	3599.9
$3.7518.10^5$ ± 1.18	128.61 ± 0.03	71.082	4211.3								
				$7.7372.10^5$ ± 2.23	115.29 ± 0.11	36.038	17130				
$2.8464.10^5$ ± 2.07	90.61 ± 0.05	42.274	5372.2	$8.3616.10^5$ ± 6.01	93.526 ± 0.44	16.374	40744	$2.6809.10^5$ ± 2.08	104.05 ± 0.07	13.467	15883
								$3.6042.10^5$ ± 1.01	84.429 ± 0.05	10.852	26500
$5.3432.10^5$ ± 1.22	61.69 ± 0.55	26.253	16239	$3.2535.10^5$ ± 7.04	77.139 ± 0.17	12.501	20766	$1.8958.10^5$ ± 2.22	72.289 ± 0.22	14.650	16654
54086 ± 3.18	57.42 ± 0.22	6.577	6561.2	$1.8455.10^6$ ± 7.11	52.445 ± 0.33	34.291	42940	$4.2989.10^5$ ± 2.03	58.908 ± 0.16	14.650	23413
$1.4540.10^5$ ± 0.07	41.23 ± 0.18	9.831	11800								
56472 ± 0.15	33.37 ± 0.06	3.519	12806								

(7)				(8)				(9)			
Area (A^j)	Center (ν^j)	Width	Height	Area (A^j)	Center (ν^j)	Width	Height	Area (A^j)	Center (ν^j)	Width	Height
$1.729.10^5$ ± 2.02	190.28 ± 0.22	33.509	4117.4								
				$1.199.10^5$ ±3.11	150.53 ± 0.08	17.774	5382.2	8069.2	168.13 ± 0.11	8.669	742.70
$2.861.10^5$ ± 1.98	126.93 ± 0.16	40.109	5691.5	$1.959.10^5$ ±2.00	118.88 ± 0.10	8.9245	4392.3				
				$3.282.10^5$ ±2.93	107.70 ± 0.09	14.025	18673	$5.732.10^5$ ± 2.22	105.88 ± 0.03	21.970	20818
				$3.999.10^5$ ±1.77	91.063 ± 0.63	10.799	29553				
$7.137.10^5$ ± 3.00	79.502 ± 0.77	33.436	17030	$3.755.10^5$ ±1.72	82.192 ± 0.22	7.8805	38028	$4.926.10^5$ ± 1.02	85.37 ± 0.04	11.853	33163
				$2.164.10^5$ ±0.77	70.675 ± 0.82	7.4978	23035	$9.624.10^5$ ± 1.93	61.88 ± 0.02	36.002	21331
$4.049.10^5$ ± 2.05	63.891 ± 0.82	10.414	31027	$1.856.10^5$ ±1.16	60.004 ± 0.10	7.0684	20955				
$4.648.10^5$ ± 2.23	52.750 ± 0.55	7.349	50470	2.4337E5	46.884 ± 0.22	10.659	18219	$2.754.10^5$ ± 0.99	42.56 ± 0.07	9.119	24104
$2.897.10^5$ ± 1.10	39.255 ± 0.10	9.820	23534	2.3414E5	43.349 ± 0.61	28.668	6516.5				
4077 ± 1.00	31.407 ± 0.03	3.261	9975.5	1.8654E5	41.057 ± 0.96	8.9245	16677				

Table 2
The straight-line plot from the regression analysis of the *n*-component mixtures; $y = A + Bx$; $N = 10$; The corresponding A^j of each of the determined compound and A^t of the modes common to each of the components in the corresponding mixtures. The shown mixtures are collected according the complex spectroscopic profile with a view to obtain the lowest *LODs* using the maximal complicated patterns, with the high level of overlapping effect and the low S/N values.

	A^j	A^t	A	B	SD	r^2	p
(1)/(5)	130.44 ± 0.08	115.03 ± 012	1.47 ± 0.08	−0.15 ± 0.01	0.1183	$\|0.9695_9\|$	<0.0001
(1)/(6)	106.12 ± 0.23	63.18 ± 0.11	19.97 ± 0.15	−2.20 ± 0.15	1.337	$\|0.9805_9\|$	<0.0001
(1)/(7)	130.38 ± 0.13	62.65 ± 0.33	30.81 ± 2.36	−3.552 ± 0.83	3.4645	$\|0.9568_4\|$	<0.0001
(1)/(8)	130.27 ± 0.52	61.17 ± 0.15	16.97 ± 0.71	−1.74 ± 0.11	1.0384	$\|0.9831_8\|$	<0.0001
(1)/(9)	130.22 ± 0.47	61.90 ± 0.14	51.27 ± 1.72	−5.36 ± 0.26	2.5158	$\|0.9894_7\|$	<0.0001
(1)/(2)/(8)	130.13 ± 0.15	151.33 ± 0.04	1.85 ± 0.26	0.51 ± 0.04	0.386	|0.973|	<0.0001
	41.44 ± 0.26	151.33 ± 0.04	57.67 ± 3.09	−6.22 ± 0.49	4.531	|0.9753|	<0.0001
(1)/(3)/(8)/(9)	130.22 ± 0.15	60.88 ± 0.99	11.88 ± 1.10	−1.10 ± 0.04	0.3914	$\|0.9939_6\|$	<0.0001
	142.22 ± 0.14	60.88 ± 0.99	7.54 ± 0.32	−0.82 ± 0.05	0.47202	|0.9845|	<0.0001

obtained data. The MLR analysis and ANOVA test data were summarized in Tables 2 and 3. The obtained concentration *LOD* of 1.47% (*LOQ*, 4.9%) indicted the perspectives for application of the THz-region for chemical identification and determination of alkaloids for the needs of forensic chemistry. The obtained concentration *LOD* of 3.4% (*LOQ* 11.333%) for the $n = 4$ components in a mixture was explained with the overlapped spectroscopic patterns of the FLs and the observed low S/N ratio. Nevertheless the concentration *LOD* (resp. *LOQ*) values were more than 2 times lower than the corresponding ones, obtained by THz-spectroscopy [1d,e]. It was important to note that in contrast to the analysis of the drugs [3i,j], where the overlapping modes, difficult the identification of each of the chemicals in the four-component mixtures, in the cases of FLs (Tables 2 and 3), at $n = 4$ were defined each of the studied components quantitatively at high confidential levels.

3.2. Validation, accuracy, measurement repeatability and precision, trueness of the measurement, reproducibility of the measurement, measurement bias and errors of the measurements, concentration limit of detection and quantification of MALDI-MS and HPLC tandem ESI–MS/MS mass spectrometric methods

The qualitative mass spectrometric analysis was performed of (2)–(7) using the fragmentation scheme typical for FLs [3,7]. In the flavone type derivatives, the B-ring was at 2-position (Scheme 1), and the MS were characterized with a peak at about *m*/*z* 117 of the cation $[C_8H_5O]^+$ with molecular weight of 117.37 [7a]. Its stability was explained with the obtained low free Gibbs energy ΔG of −134.16 kcal/mol. In flavone type NPs, the common fragmentation scheme was given in Fig. 3. Typically a fragmentation peak of the $[C_7H_5O_3]^+$ cation with the peak at about *m*/*z* 137 was observed [3,7], characterizing $\Delta G = -110.32$ kcal/mol, also proposed a high

Table 3
Multiple Regression Analysis and ANOVA test the data in Table 1 for the $v_i^{(j)}$ and $Av_i^{(j)}$; The Prob. *F* value for all calculations is <0.0001.

Value	Std. Error	*t*-Value	Prob (>|*t*|)	r^2	ESD		*df*	SS	MS	*F* Statistic	Prob F
(1)/(5)											
0	–	–	<0.0001	0.96959	0.7291	Model	1	−2.9155	−2.9154	−5.4842	<0.0001
0.0650	0.0372	1.7496	<0.0001			Error	9	4.7845	0.5316		
							10	1.8691			
(1)/(6)											
0	–	–	–	0.98059	11.9243	Model	1	−907.7916	−907.7915	−6.3844	<0.0001
1.2211	0.7821	1.5613	<0.0001			Error	9	1279.6994	142.1888		
							10	371.9078			
(1)/(7)											
0	–	–	<0.0001	0.95684	15.3845	Model	1	−993.2421	−993.2421	−4.1965	<0.0001
0.8494	0.7841	1.0834	<0.0001			Error	9	2130.1432	236.6825		
							10	1136.9010			
(1)/(8)											
0	–	–	–	0.98318	8.3398	Model	1	−367.4456	−367.4455	−5.2830	<0.0001
0.6843	0.4250	1.5613	<0.0001			Error	9	625.9702	69.5522		
							10	258.5247			
(1)/(9)											
0	–	–	–	0.98947	25.1310	Model	1	−3266.1223	−3266.1223	−5.1714	<0.0001
1.9679	0.9791	1.2808	<0.0001			Error	9	5684.1078	631.5675		
							10	2417.9855			
(1)/(2)/(8)											
				0.97299	0.9707	Model	1	13.8363	13.8363	14.6833	0.00402
0			<0.0001			Error	9	8.4808	0.9423		
0.7696	0.0495	15.5557	<0.0001			Total	10	22.3172			
				0.9753	28.4641	Model	1	−3926.0342	−3926.0342	−4.8457	<0.0001
0			<0.0001			Error	9	7291.8277	810.2030		
2.0095	1.4507	1.4507	<0.0001			Total	10	3365.7935			
(1)/(3)/(8)/(9)											
				0.99396	5.8069	Model	1	−201.753	−201.753	−5.9830	<0.0001
0			<0.0001			Error	9	303.4868	33.7207		
0.5929	0.2959	2.0034	<0.0001			Total	10	101.7338			
				0.9845	1.3371	Model	1	−65.7851	−65.7852	−4.7857	<0.0001
0			<0.0001			Error	9	123.715	13.7461		
0.252	0.1890	1.3371	<0.0001			Total	10	57.9298			

Table 4
Area ratios (AR) versus the concentration (C, ng) of the performed mass spectrometric calibration measurements of **(2)**; The data of three repeated measurements and three times determination of the corresponding quantities were analized. The linear plots, *r*, *p*, parameters (*a* and *b*), and standard deviation (SD) data were given for $N = 11$ number of points.

AR	C			AR	C			AR	C		
$x_{1,1}$	$y_{1,1}$	$y_{1,2}$	$y_{1,3}$	$x_{1,2}$	$y_{2,1}$	$y_{2,2}$	$y_{2,3}$	$x_{1,3}$	$y_{3,1}$	$y_{3,2}$	$y_{3,3}$
2.7651 ± 0.14	5.0031 ± 0.02	5.0029 ± 0.07	5.0030 ± 0.29	2.7658 ± 0.02	5.0028 ± 0.02	5.0028 ± 0.01	5.0027 ± 0.08	2.7650 ± 0.01	5.0030 ± 0.07	5.0030 ± 0.02	5.0028 ± 0.00
1.3321 ± 0.03	2.5056 ± 0.01	2.5051 ± 0.13	2.5052 ± 0.18	1.3320 ± 0.01	2.5055 ± 0.01	2.5051 ± 0.02	2.5051 ± 0.09	1.3323 ± 0.02	2.5055 ± 0.13	2.5050 ± 0.16	2.5051 ± 0.02
1.0683 ± 0.07	1.8992 ± 0.10	1.8990 ± 0.09	1.8991 ± 0.33	1.0683 ± 0.02	1.8990 ± 0.72	1.8989 ± 0.04	1.8990 ± 0.02	1.0682 ± 0.10	1.8991 ± 0.28	1.8989 ± 0.33	1.8990 ± 0.00
0.3652 ± 0.10	0.6334 ± 0.17	0.6333 ± 0.55	0.6335 ± 0.16	0.3651 ± 0.06	0.6334 ± 0.01	0.6323 ± 0.01	0.6332 ± 0.01	0.3652 ± 0.22	0.6333 ± 0.67	0.6332 ± 0.18	0.6334 ± 0.07
2.7101 ± 0.22	5.1000 ± 0.08	5.0987 ± 0.08	5.0999 ± 0.90	2.7188 ± 0.01	5.0993 ± 0.00	5.0984 ± 0.02	5.0988 ± 0.10	2.7100 ± 0.11	5.0900 ± 0.61	5.0988 ± 0.27	5.0998 ± 0.02
1.5822 ± 0.15	2.8808 ± 0.10	2.8810 ± 0.01	2.8811 ± 0.25	1.5820 ± 0.01	2.8807 ± 0.02	2.8802 ± 0.11	2.8810 ± 0.55	1.5820 ± 0.13	2.8810 ± 0.53	2.8809 ± 0.19	2.8810 ± 0.05
1.0950 ± 0.01	1.9887 ± 0.09	1.9885 ± 0.02	1.9888 ± 0.15	1.0948 ± 0.07	1.9885 ± 0.09	1.9882 ± 0.18	1.9887 ± 0.18	1.0945 ± 0.18	1.9885 ± 0.10	1.9884 ± 0.25	1.9887 ± 0.08
0.4932 ± 0.05	0.9873 ± 0.07	0.9872 ± 0.01	0.9874 ± 0.47	0.4931 ± 0.09	0.9871 ± 0.88	0.9871 ± 0.16	0.9873 ± 0.44	0.4931 ± 0.22	0.9872 ± 0.22	0.9871 ± 0.28	0.9873 ± 0.19
0.5031 ± 0.07	0.9812 ± 0.22	0.9813 ± 0.06	0.9813 ± 0.44	0.5030 ± 0.36	0.9810 ± 0.01	0.9812 ± 0.05	0.9811 ± 0.21	0.5030 ± 0.33	0.9813 ± 0.19	0.9812 ± 0.33	0.9812 ± 0.22
2.7653 ± 0.04	5.0803 ± 0.26	5.0801 ± 0.15	5.0802 ± 0.50	2.7652 ± 0.14	5.0802 ± 0.01	5.0800 ± 0.01	5.0802 ± 0.02	2.7652 ± 0.45	5.0802 ± 0.23	5.0801 ± 0.17	5.0801 ± 0.50
2.7883 ± 0.01	5.1115 ± 0.70	5.112 ± 0.34	5.1119 ± 0.05	2.7883 ± 0.40	5.1114 ± 0.02	5.1118 ± 0.17	5.1122 ± 0.07	2.7883 ± 0.67	5.1114 ± 0.09	5.1110 ± 0.90	5.1112 ± 0.04
Linear plot data of the dependences $x_{i,j}$ versus $y_{i,j}$ ($i,j = 1–3$)											
Parameters	Value	Error		Parameters	Value	Error		Parameters	Value	Error	
a	0.0141_4	0.0390_7		*a*	0.0157_1	0.0372_9		*a*	0.0152	0.0378_9	
b	1.8328_2	0.0211_1		*b*	1.8308_2	0.0201_4		*b*	1.8316_6	0.0204_9	
r	SD	*N*	*p*	*r*	SD	*N*	*p*	*r*	SD	*N*	*p*
0.9994	0.0665	11	<0.0001	0.9994_6	0.0635_1	11	<0.0001	0.9994_4	0.0645	11	<0.0001
Parameters	Value	Error		Parameters	Value	Error		Parameters	Value	Error	
a	0.0141	0.0389_2		*a*	0.0153_9	0.0372_7		*a*	0.0142_8	0.0388_9	
b	1.83273	0.0210_3		*b*	1.8308_9	0.0201_3		*b*	1.8326_5	0.0210_2	
r	SD	*N*	*p*	*r*	SD	*N*	*p*	*r*	SD	*N*	*p*
0.9994_1	0.0662_5	11	<0.0001	0.9994_6	0.0634_7	11	<0.0001	0.9994_1	0.0662_1	11	<0.0001
Parameters	Value	Error		Parameters	Value	Error		Parameters	Value	Error	
a	0.0141_9	0.0390_4		*a*	0.0157_1	0.0372_3		*a*	0.0143_7	0.0390_1	
b	1.8328_1	0.0211		*b*	1.8308_4	0.0201_1		*b*	1.8327_1	0.0210_8	
r	SD	*N*	*p*	*r*	SD	*N*	*p*	*r*	SD	*N*	*p*
0.9994	0.0664_5	11	<0.0001	0.9994_6	0.0634	11	<0.0001	0.9994_1	0.0664	11	<0.0001

Table 5
Statistical tests (MLR and ANOVA) of the obtained HPLC-ESI/MS-MS experimental data of **(2)** (Table 4 of the three repeated measurements, of three samples of same compound, measured consequently under same experimental conditions, where the presented data of AR were obtained by the three repeated computational procedures.

Parameter	Value	Error	*t*-value	Prob (>|*t*|)	r^2	ESD
y-Intercept	-0.0019_7	0.0200_3	-0.0985_6	0.9242_5	0.9992_1	0.0333_9
K	-9.4417_4	49.7461_9	−0.1898	0.8548_5		
L	58.0640_3	32.6076_5	1.7806_9	0.1181_8		
M	-48.0745_8	65.9254_9	-0.7292_3	0.4895_4		
	df	SS	MS	*F* Statistic		Prob F
Model	3	9.91311	3.30437	2963.6292_3		<0.0001
Error	7	0.0078	0.00111			
Total	10	9.9209_2				
Parameter	Value	Error	*t*-value	Prob (>|*t*|)	r^2	ESD
y-Intercept	-0.0105_2	0.0267_8	-0.3930_2	0.7060	0.99894	0.0387_1
I	-27.7871_3	34.9912_1	-0.7941_2	0.4532		
J	−11.7942	37.2188_6	-0.3168_9	0.7605_7		
E	40.1263_7	46.4038_6	0.8647_2	0.4158_4		
	Df	SS	MS	F Statistic		Prob *F*
Model	3	9.9104_3	3.3034_8	2204.2927_9		<0.0001
Error	7	0.0104_9	0.0015			
Total	10	9.9209_2				
Parameter	Value	Error	*t*-value	Prob (>|*t*|)	r^2	ESD
y-Intercept	-0.0113_2	0.0232	-0.4880_4	0.6404_4	0.9993_2	0.0311_4
G	6.9149_3	8.6047_6	0.8036_2	0.4480_4		
C	11.8236_7	79.1017_3	0.1494_7	0.8853_9		
D	-18.1890_7	71.3565	−0.2549	0.8061_2		
	df	SS	MS	*F* Statistic		Prob F
Model	3	9.9141_3	3.3047_1	3407.3972_4		<0.0001
Error	7	0.0067_9	$9.6986.10^{-4}$			
Total	10	9.9209_2				
Parameter	Value	Error	*t*-value	Prob (>|t|)	r^2	ESD
y-Intercept	0.0018	0.0214_7	0.0838_4	0.9467_5	0.9999	0.00123
K	-7.6850_9	82.5279_8	-0.0931_2	0.9408_9		
L	-2.1603_9	11.7596_8	-0.1837_1	0.8843_4		
M	-1.1566_7	45.7468_9	-0.0252_2	0.9839_1		
H	2.6277	30.8637_1	0.0851_4	0.9459_3		
I	6.2730_3	75.0289_6	0.0836_1	0.9469		
J	0.7196_6	7.7189_5	0.0932_3	0.9408_2		
E	2.1442_7	28.2998	0.0757_7	0.9518_6		
F	-1.6293_9	30.9077_9	-0.0527_2	0.9664_7		
G	1.8657_8	20.1219_6	0.0927_2	0.9411_4		
	df	SS	MS	*F* Statistic		Prob *F*
Model	9	9.9209_2	1.1023_2	724825.6020_3		
Error	1	$1.5208.10^{-6}$	$1.5208.10^{-6}$			
Total	10	9.9209_2				

Table 6
Statistical tests (MLR and ANOVA) of the otained HPLC-ESI/MS-MS experimental data of **(2)**, prepared as standard and the measurements of the extract of the natural extract of (**2**) of the three repeated measurements, of three samples of same compound, measured concequently under same experimental conditions, where the presented data of AR were obtained by the three repeated computational procedures.

AR	C		
$x_{1,4}$	$y_{4,1}$	$y_{4,2}$	$y_{4,3}$
2.7400 ± 0.34	5.0018 ± 0.22	5.0026 ± 0.18	5.0030 ± 0.02
1.3339 ± 0.11	2.5038 ± 0.52	2.5041 ± 0.36	2.5042 ± 0.34
1.0570 ± 0.02	1.8772 ± 0.16	1.8989 ± 0.29	1.8988 ± 0.02
0.3432 ± 0.01	0.6301 ± 0.17	0.6332 ± 0.67	0.6332 ± 0.00
2.7061 ± 0.66	5.0183 ± 0.44	5.0182 ± 0.03	5.0181 ± 0.03
1.5833 ± 1.26	2.8851 ± 0.23	2.8888 ± 0.08	2.8877 ± 0.06
1.0962 ± 0.32	1.7621 ± 0.12	1.9881 ± 0.69	1.9880 ± 0.18
0.4922 ± 0.98	0.984 ± 0.01	0.9870 ± 0.17	0.9830 ± 0.33
0.5029 ± 0.90	0.9812 ± 0.08	0.9812 ± 0.15	0.9812 ± 0.93
2.7648 ± 0.02	5.0854 ± 0.62	5.0854 ± 0.33	5.0853 ± 0.90
2.7873 ± 0.05	5.1111 ± 0.58	5.1110 ± 0.01	5.1110 ± 0.16

Parameter	Value	Error	*t*-value	Prob (>|*t*|)	r^2	*ESD*
y-Intercept	0.0147_4	0.0073_7	2.0001_3	0.0924_1	0.9999_4	0.0095_4
D	0.1178_3	0.1454_8	0.8099_5	0.4488_9		
O	1.3243_4	0.1684_6	7.8612_2	$2.2418.10^{-4}$		
P	0.0741_2	0.0508_2	1.4586_6	0.1949_4		
N	-0.3706_6	0.2282_2	-1.6241_6	0.1554_7		
	df	SS	MS	*F* Statistic		Prob *F*
Model	4	9.9203_7	2.4800_9	27224.7927_3		<0.0001
Error	6	$5.4658.10^{-4}$	$9.1097.10^{-5}$			
Total	10	9.9209_2				

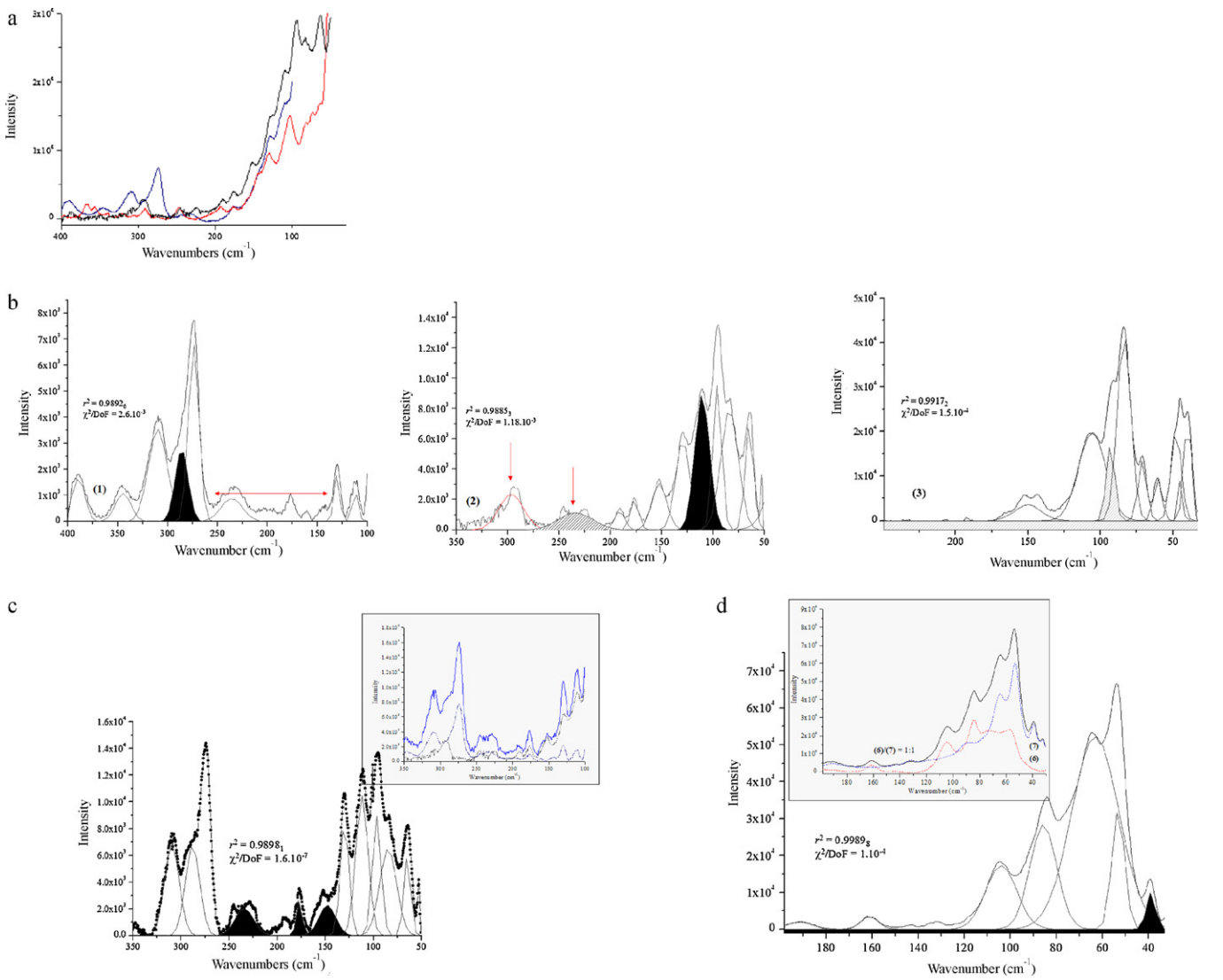

Fig. 1. The solid-state Raman spectra of (1) (blue solid line), (2) (black solid line) and (9) (red solid-line) within the 400–30 cm^{-1} spectroscopic region (a); Curve-fitted solid-state Raman spectra within the 200–30 cm^{-1} of the isolated FLs (b) the solid-mixtures at molar ratio (1):(2):(9) = 1:1:1 (c) and (6):(7) = 1:1 (d) curve-fitted spectroscopic patterns after the baseline correction method, by non-linear multipeak Lorenzian–Gaussian function at ratio 1:1; *A*- total area under the curve from the baseline center of the peak; w^2 "sigma", approximately 0.5 the FWHM; $w/2$ - is the standard deviation, respectively. (For interpretation of the references to color in this figure legend, the reader is referred to the web version of this article.)

stability of the fragment in ionization gas-conditions. The mass spectrometric data of the mixture **(1)/(3)** depicted in Fig. 3a were associated with the fragmentation of the flavonoid skeleton as shown. The peaks at about *m*/*z* 269, 180, 159, 133 and 107 were assigned the **(3)**, while the corresponding ones at about *m*/*z* 433, 238 to **(1)**, respectively (Fig. 3a). The series of peaks at about *m*/*z* 137 were common for both compounds. To the carbohydrate fragment in (**1**) could be associated the peaks at about *m*/*z* 134, and 120, similar to the previously reported MS data of other derivatives [3,7]. Interestingly were the observed peaks at *m*/*z* 270.01 and 270.34 in the *n*-component mixtures in the presence of **(1)** (Fig. 3b). Since the fragmentation of the carbohydrate moiety, lead to the stabilization of the cationic $[C_{15}H_{11}O_6]^+$ fragment with molecular weight of 287.248. The peak at about *m*/*z* 270 could be associated with the $[M^+]–H_2O$ ($[C_{15}H_{10}O_5]^+$, 270.241), respectively (Fig. 3). Since such species were found only in the MALDI MS data, their formation could be assigned as result the non-covalent interactions of the alkaloids in the crystalline DHB-matrix/matrix-analyte sample. A confirmation of this assumption followed by the observed peaks at *m*/*z* 587.25 assigned to the DHB-**(1)** associate stable in gas phase. In a similar way could be assigned the peak at *m*/*z* 470.33 to DHB-**(8)**, respectively. The stabilization of different resonance forms of FLs, depending the pH in the presence the DHB, independently of the relatively weak acidic properties of the matrix, should also taking into account, interpretation the MALDI-MS data. Moreover the theoretical DFT calculations showed that the proposed proton transfer, stabilized species of type, depicted in Fig. 3, characterizing $\Delta G = (-234.65)$ to (-310.44) kcal/mol, respectively.

The correlations between the results in samples with different amounts of (1)–(9) for all of studied systems, obtained by spectroscopic Raman method (Table 2) and the parallel HPLC-ESI MS/MS technique demonstrate good agreement with correlation coefficients > 0.99973. HPLC-ESI MS/MS analyses of the isolated compounds were performed using the procedures described for quantitative determination [7]. The corresponding *m*/*z* values of each of the samples in the isolated components as well as at the mixtures show similar fragmentation schemes using both the ESI–MS and MALDI MS methods.

The calibration and validation of the HPLC-ESI–MS/MS method were performed for the parallel quantification. The calibration

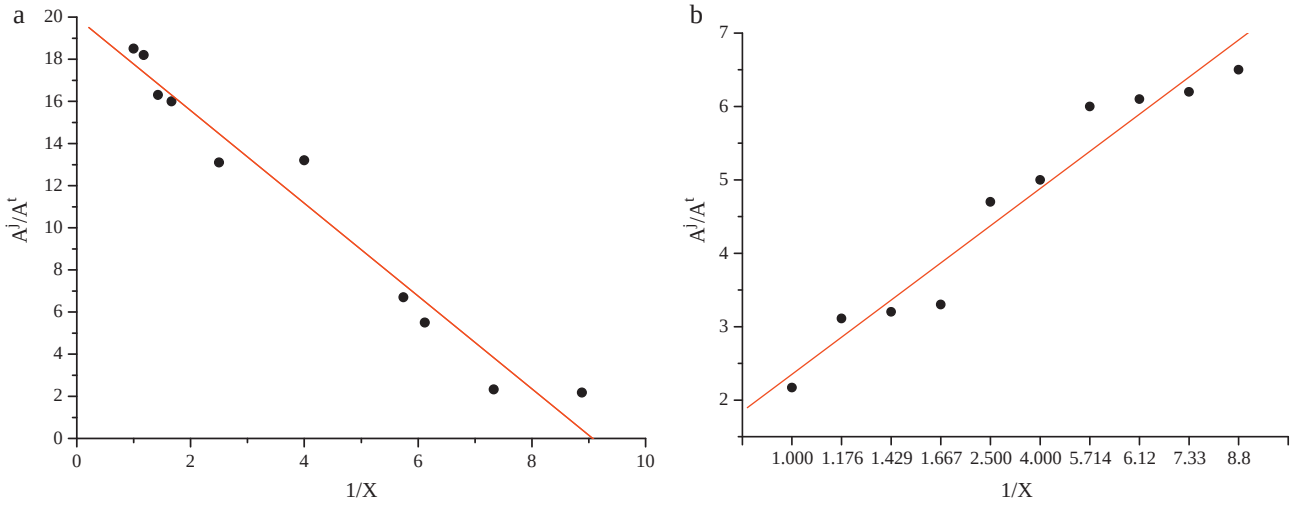

Fig. 2. The straight-line plot from the regression analysis of the different component mixtures, i.e. (1)/(6) = 1:1 (a) and (1)/(2)(8) = 1:1:1 (b), determining the component (1); The corresponding area of the A^j belonging to (1) to the area peak A^t of the common for the all components mode in the solid-state Raman spectra with the obtained linear equation parameters collected in Table 2; the obtained MLR and ANOVA data are summarized in Table 3, respectively.

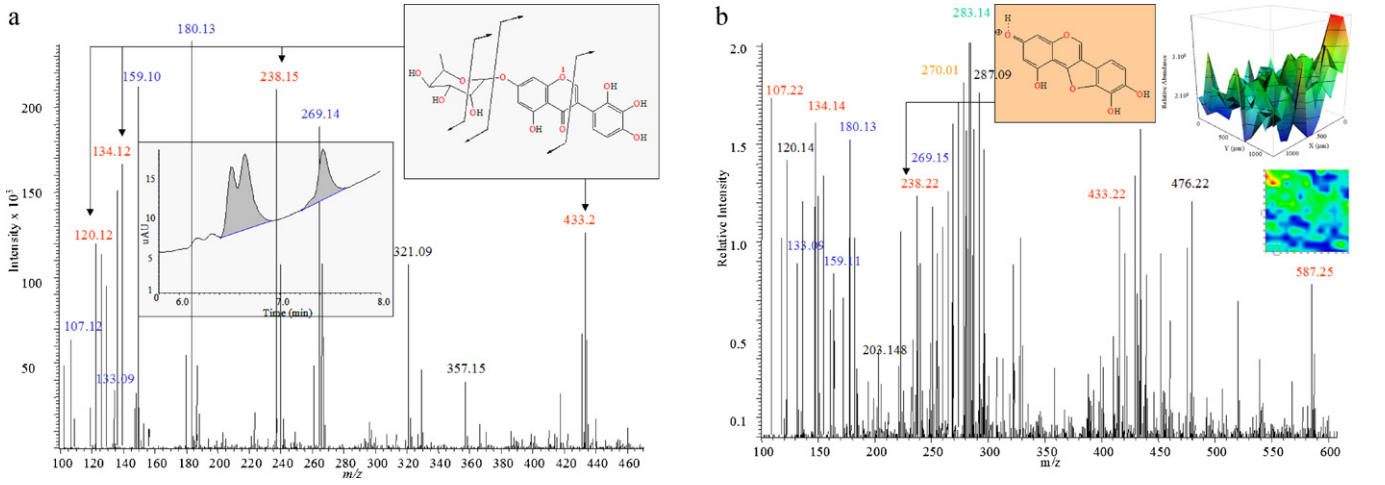

Fig. 3. ESI–MS and mass chromatogram (small figure) of the mixture (1)/(3) at molar ratio 1:1 (a) (the peaks of the fragments of (1) are shown in red, while to the (3) corresponds the peaks given in blue); as well as MALDI-MS data with the corresponding 3D and 2D images by logarithm ploting of Δx, Δy vs. the signal amplitude (grid) of selected ion range (small figures) for the (1) (b), respectively; the Fragmentation scheme and chemical diagram of (1); The peak at 283.14 (green) belongs to the standard. (For interpretation of the references to color in this figure legend, the reader is referred to the web version of this article.)

standard plot was depicted in Fig. 4 and summarized in Table 4. The obtained MLR analysis and ANOVA for the three repeated measurements and determination of the area ratio (AR) as well as concentration (C), were summarized in the same Tables 4 and 5, respectively. The obtained r^2 values were within 0.9994–0.99946, respectively. The accuracy, and repeatability condition of measurements, was evaluated by the presented data in Tables 4 and 5, respectively. The trueness of measurement was evaluated, using the prepared standard of (**2**), and performed statistical analysis of the obtained data of natural extract of (**2**) in mixture (Table 6). The presented data for the y-intercept parameters were labelled according the following matrix:

$$\begin{array}{cccc} A(x_{1,1}) & K(y_{1,1}) & L(y_{1,2}) & M(y_{1,3}) \\ H(x_{2,1}) & I(y_{2,1}) & J(y_{2,2}) & E(y_{2,3}) \\ F(x_{3,1}) & G(y_{3,1}) & C(y_{3,2}) & D(y_{3,3}) \\ O(x_{4,1}) & P(y_{4,1}) & N(y_{4,2}) & B(y_{4,3}) \end{array}$$

The data in Table 6 show the r^2 within 99994–99.99% confidence of the data.

3.3. Electronic transitions and optical spectra

The physical optical properties, of the FLs, were elucidated by the theoretical analysis of the non-substituted common molecular fragments (I)–(III) [3] (Scheme 1 and Fig. 5). The solvent accessible surfaces (Scheme S1), dispersion, repulsion and Gibbs free energy as well as the total dipole moments (μ_{tot}) were evaluated. The protonation ability was quantified by the NBO singly charges q_X(NBO) (X = N, O). The data were summarized in Tables S2 and S3, respectively. The precision of our theoretical data were evaluated, using R(+)-, L(-)- and R,L-enantiomers of chiral molecule, 1-phenylethylamine as standard. The protonation ability was quantified, using the synthetic organic salt ***Sd*-(*1*)**. The obtained difference between the theoretical and experimental data of 1.1 ± 0.046 nm (Fig. 3) is an excellent correlation. The theoretical data for the (**I**) and (**II**) show λ_{max} at about 325, 310 and 285 nm (Table 5). Depending of the substituents (–OH and/or –OCH_3), a bathochromic shift about 5–9 nm was obtained. The (**III**) was characterized with λ_{max} at 355, 315 and 310 nm. The obtained untypical shifting to the higher wavelengths could explain only with the

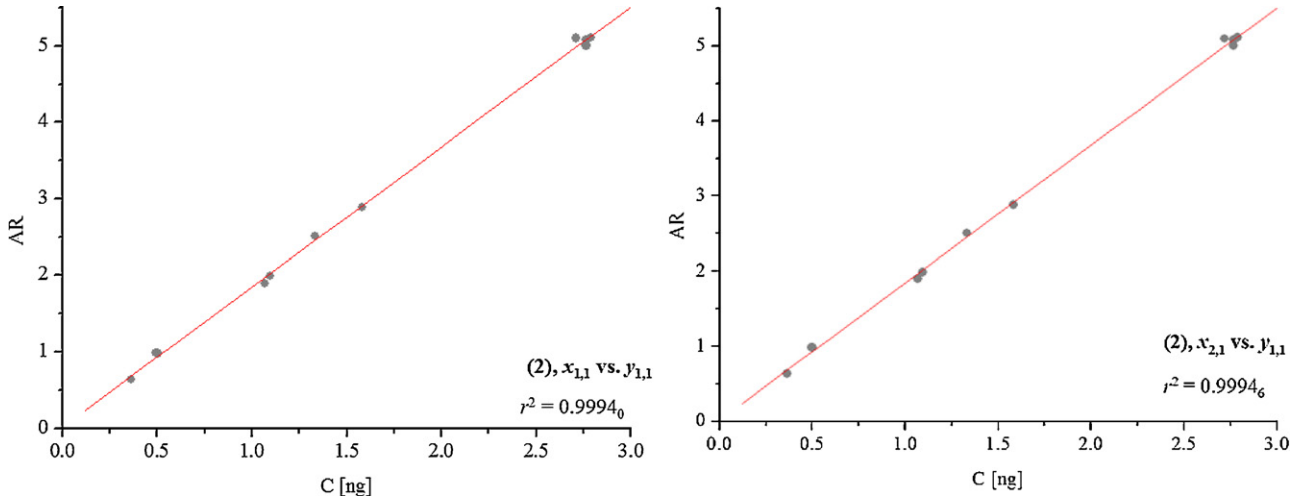

Fig. 4. The calibration dependence of the area ratio (AR) versus the concentration (*C*, [ng]) of the (2), obtained by the HPLC-ESI–MS/MS experiment (Tables 4 and 5).

intramolecular H–π interaction (3.672_2 Å). The μ_{tot} of (**I**) and (**II**) were found within 3.5605–4.24. The corresponding one of (**III**) was found 3.5605, respectively. The resonance forms (**Ia**), (**Ib**), and (**IIb**), characterizing with higher μ_{tot} quantities were stabilized in polar protic solvents. In contrast the (**IIIa**), showing lower μ_{tot} quantity. Remarkably were the obtained values for λ_{max} of last forms characterizing with the λ_{max} of about 25–116 nm batochromically shifted. This result allows their unambiguously defining in the metabolites, depending of the solvent polarity, as experimentally was proven by the obtained data of λ_{max} and $[\alpha]_D$ (Table 5) [6,7]. Thus a difference of about 2.5–6 nm was found. The performed mathematical procedure for the smoothing of the patterns in Fig. 4 using the SG method and FFT at different polynomial functions leads to the confidence levels within 99.3–98.6%, so as to verify the absence of statistically significant differences. A critical discussion however of the capability of the method for the needs of the forensic chemistry in general

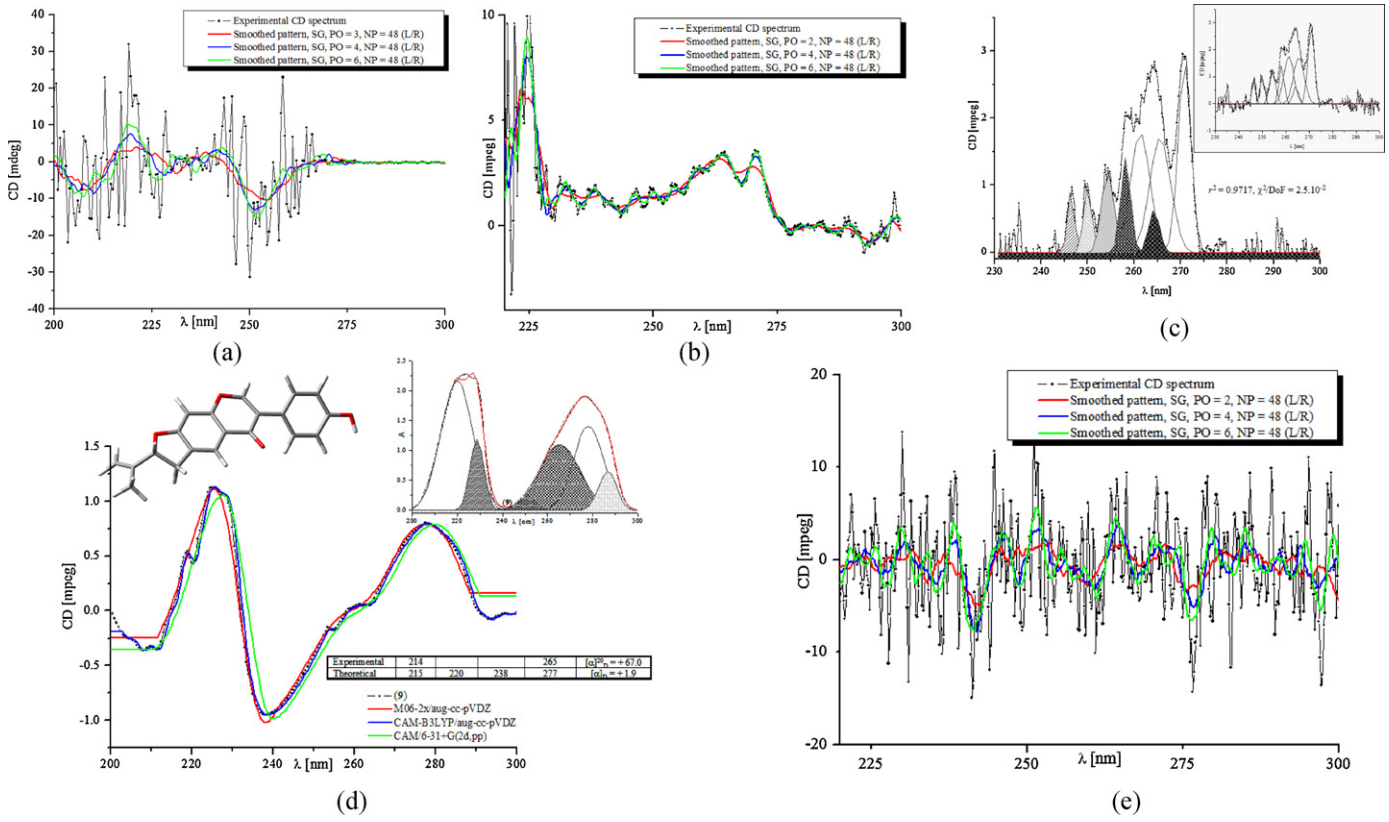

Fig. 5. Experimental CD spectra in methanol at concentration 2.10^{-4} mol/l S- and R-enantiomers of the standard (a,b) and ***Sd-(1)*** (c); experimental electronic absorption and CD spectra of (**9**) as well as the obtained most stable conformers in solution and (d) nonlinear curve-fitted spectroscopic patterns by multipeak Gaussian function after applied baseline correction method; *A*- total area under the curve from the baseline center of the peak; w^2 "sigma", approximately 0.745 the FWHM; $w/2$ - is the standard deviation; Smooted spectroscopic pattern by the Savitzky–Golay (SG) method at different polynomial orders (PO) and left-right side (L/R), number of points (NP). Experimental CD spectra in methanol at concentration 2.10^{-4} mol/l of L,R-enantiomeric mixture of the standard; Smooted spectroscopic pattern by the Savitzky–Golay (SG) method at different polynomial orders (PO) and left-rigth side (L/R), number of points (NP) (e).

requires evaluating the possibility of the method for analysis of mixtures. Nevertheless the concentration *LOD* of 10^{-6} mol/l was found, the strong overlapping character of the absorption maxima and the broad band profile as well as low effect of the substituents on the λ_{max}, difficult in significant level the wide application of the method for quantitative analysis.

4. Conclusions and outlook

The main aim of the paper was to illustrate the perspectives and capability of the complementary application of the solid-state Raman method within the THz-region and the mass spectrometric methods and techniques for analysis of the crystalline samples. The obtained metrological data about accuracy, measurement repeatability and precision, trueness of the measurement, reproducibility of the measurement, concentration limit of detection and quantification for series of nine flavonoids and their multicomponent mixtures allow further development of fast analytical tests, creating the protocols and databases for accurate both qualitative and quantitative analysis of the natural alkaloids, including as well semi- and synthetic analogous. Since a concentration *LOD* 1.42% (resp. *LOQ*, 4.766%) for the quantified component in a four-component mixture, were achieved by the Raman spectroscopy, the concentration *LOD* of 10^{-7} mol/l (*LOQ*, $3.666.10^{-7}$ mol/l) of the analyte was obtained by MALDI-MS method, as well as the obtained data for thetrueness of the measurements, using the statistically evaluated data from the analysis of the standard and natural mixture of flavonoids, giving 99.99% confidence level, were of importance for the fields of natural products research and analysis of unknown alkaloids in natural extracts, semi-synthetic and synthetic mixtures; for drugs-design and pharmaceutical analysis and well as for the needs the forensic chemistry and casework.

5. Supplementary material

Experimental section; Details on the statistical analysis and mathematical tools (Chemometrics), Crystallographic data (Table S1); Conformational analysis (Fig. S1); The solvent accessible surface; r_{max}, r_{min} – maxima, respectively, minimal distribution between center of nuclear charge and isosurface; S_{tot} – total solvent accessible surface area of solute, V – volume of solute cavity; E_{cav} – cavitation energy, E_d – dispersion energy, E_r – repulsion energy, ΔG_{solv}– Gibbs free energy, and μ_{tot} – total dipole moment (Scheme S1); Theoretical q_X(NBO) charges at $X = N$ and/or O depending of the polarizable continuum model (Table S2) and theoretical and experimental data of the electronic absorption spectra and ORs (Table S3).

Acknowledgements

The authors thank the Deutscher Akademischer Austausch Dienst (DAAD), for a grant within the priority program "Stability Pact South-Eastern Europe" and the Deutsche Forschungsgemeinschaft (DFG) for Grants SPP 255/21-1 and SPP/22-1. The authors also thank the central instrumental laboratories for structural analysis at Dortmund University of Technology (TUD, Germany) and the analytical and computational laboratories at the Institute of Environmental Research (INFU) at the TUD.

Appendix A. Supplementary data

Supplementary data associated with this article can be found, in the online version, at doi:10.1016/j.talanta.2011.12.016.

References

[1] (a) K. Siebert, K. Löffler, H. Quast, M. Thomson, T. Bauer, R. Leonhardt, S. Czasch, H. Roskos, Phys. Med. Biol. 47 (2002) 3743–3748;
(b) S. Wietzke, C. Jansen, F. Rutz, D. Mittleman, M. Koch, Polym. Test 26 (2007) 614–618;
(c) M. Theuer, R. Beigang, D. Grischkowsky, Appl. Phys. Lett. 96 (2010) 191110;
(d) A. Redo-Sanchez, G. Salvatella, R. Galceran, L. Roldos, J. Garcia-Reguero, M. Castellari, J. Tejada, Analyst 136 (2011) 1733–1768;
(e) Y. Chen, Y. Ma, Z. Lu, B. Peng, Q. Chen, J. Appl. Phys. 110 (2011) 044902.
[2] (a) L. Kobilinsky, (Hrsg.) Forensic Chemistry Handbook, Wiley, 2011;
(b) J. Winefordner, J. Almirall, Forensic Chemistry (Chemical Analysis: A Series of Monographs on Analytical Chemistry), J. Wiley and Sons, 2012;
(c) L. Sorensen, J. Chromatogr. B 879 (2011) 11–12;
(d) S. Darby, M. Miller, R. Allen, J. Forens. Sci. 46 (2001) 1033–1042;
(e) E. Bartick, Applications of vibrational spectroscopy in criminal forensic analysis, in: J. Chalmers, P Griffiths (Eds.), Handbook of Vibrational Spectroscopy, vol. IV, J. Wiley & Sons Ltd., Chichester, 2002;
(f) E. Suzuki, Forensic applications of infrared spectroscopy, in: R. Saferstein (Ed.), Forensic Science Handbook, vol. III, Prentice-Hall, New York, 1993, pp. 71–195;
(g) E. Bartick, M. Tungol, Infrared microscopy and its forensic applications, in: R. Saferstein (Ed.), Forensic Science Handbook, vol. III, Prentice-Hall, New York, 1993, pp. 196–252;
(h) E. Bartick, M. Tungol, J. Reffner, Anal. Chim. Acta 288 (1994) 35–42.
[3] (a) S. Kusari, M. Spiteller, Nat. Prod. Rep. 28 (2011) 1203–1207;
(b) S. Puri, V. Verma, T. Amna, C. Qazi, M. Spiteller, J. Nat. Prod. 68 (2005) 1717–1719;
(c) M. Awouafack, P. Spiteller, M. Lamshöft, S. Kusari, B. Ivanova, P. Tane, M. Spiteller, J. Nat. Prod. 74 (2011) 272–278;
(d) B. Kindler, H. Krämer, S. Nies, P. Gradicsky, G. Haase, P. Mayser, M. Spiteller, P. Spiteller, Eur. J. Org. Chem. 11 (2010) 2084–2090;
(e) H. Zhang, I. Oppel, M. Spiteller, K. Günther, G. Böhmler, S. Zühlke, Chirality 21 (2009) 271–275;
(f) B. Ivanova, M. Spiteller, J. Mol. Struct. 104 (2011) 303–312;
(g) B. Ivanova, M. Spiteller, Biopolymers 97 (2011) 134–144;
(h) B. Ivanova, M. Spiteller, Nat. Prod. Commun. 7 (2012) 1–8;
(i) M. Lamshoft, B. Ivanova, M. Spiteller, Talanta 85 (2011) 2562–2575;
(j) B. Ivanova, M. Spiteller, J. Pharmaceut. Biomed. Anal. doi:10.1016/j.jpba.2011.10.028;
(k) J. Harborne, C. Williams, Nat. Prod. Rep. 12 (1995) 639–657;
(l) N. Veitch, R. Grayer, Nat. Prod. Rep. 25 (2008) 555–611;
(m) N. Veitch, Nat. Prod. Rep. 26 (2009) 776–802;
(n) N. Veitch, R. Grayer, Nat. Prod. Rep. (2011), DOI: 10.1039/c1np00044f;
(o) F. Liu, H. Gu, X. Yuan, X. Dong, Appl. Spectrosc. 64 (2010) 1301–1306.
[4] (a) G.M. Sheldrick, A64 (2008) 112–122;
(b) G.M. Sheldrick, D66 (2010) 479–485;
(c) G.M. Sheldrick, A46 (1990) 467–473;
(d) A. Spek, 36 (2003) 7–13.
[5] (a) http://de.openoffice.org/;
(b) C. Kelley, SIAM Front. App. Math. (1999) 18–27;
(c) K. Madsen, H. Nielsen, O. Tingleff, Informatics and Mathematical Modelling, 2nd ed., DTU Press, 2004;
(d) P. Stephens, D. McCann, J. Cheeseman, M. Frisch, Chirality 17 (2005) S52–S54;
(e) A. Yildiz, P. Selvin, Acc. Chem. Res. 38 (2005) 574–585;
(f) D. Marquardt, J. Soc. Ind. Appl. Math. 11 (1963) 431–441;
(g) P. Griffiths, G. Pariente, Trends Anal. Chem. 5 (1986) 205–209;
(p) D. Crawford, Theor. Chem. Acc. 115 (2006) 227–245;
(h) J. Al-Zoubi, S. Koundourellis, S. Malamataris, J. Pharm. Biomed. Anal. 29 (2002) 459–467;
(i) T. Pfeifer, J. Tuerk, K. Bester, M. Spiteller, Rapid Commun. Mass Spectrom. 16 (2002) 663–669.
[6] (a) Dalton 2.0 Program Package; http://www.daltonprogram.org/download.html;
(b) F. De Proft, P. Geerlings, Chem. Rev. 101 (2001) 1451–1464;
(c) M. Dolg, U. Wedig, H. Stoll, H. Preuss, J. Chem. Phys. 86 (1987) 866;
(d) M. Frisch, et al. Gaussian 09, Gaussian, Inc., Pittsburgh, PA, 1998.;
(e) GausView03; http://www.gaussian.com/g_prod/gv3.htm;
(f) S. Grimme, A. Bahlmann, G. Haufe, Chirality 14 (2002) 793–797;
(g) W. Hehre, L. Radom, S. Schleyer, J. Pople, J. Ab Initio Molecular Orbital Theory, Wiley, New York, 1986;
(h) B. Ivanova, M. Spiteller, J. Phys. Chem. A 114 (2010) 5099–5103;
(i) B. Ivanova, M. Spiteller, Cryst. Growth Des. 10 (2010) 2470–2473;
(j) B. Ivanova, M. Spiteller, M. Biopolymers, 93 (2010) 727–734;
(k) Y. Zhao, D. Truhlar, Accts. Chem. Res. 41 (2008) 157–167;
(l) Y. Zhao, D. Truhlar, Theor. Chem. Acc. 120 (2008) 215–241.
[7] (a) R. Hughes, T. Croley, C. Metcalfe, R. March, Int. J. Mass Spectrom. 210/211 (2001) 371–385;
(b) F. Cuyckens, M. Claeys, J. Mass Spectrom. 39 (2004) 1–15;
(c) F. Ferreres, R. Llorach, A. Gil-Izquierdo, J. Mass Spectrom. 39 (2004) 312–321;
(d) F. Cuyckens, M. Claeys, J. Mass Spectrom. 40 (2005) 364–372;
(e) F. Cuyckens, R. Rozenberg, E. Hoffmann, M. Claeys, J. Mass Spectrom. 36 (2001) 1203–1210;
(f) J. Yinon, D. Issachar, H. Boettger, Org. Mass Spectrom. 13 (1978) 167–171;
(g) L. Abrankó, J. García-Reyes, A. Molina-Díaz, J. Mass Spectrom. 46 (2011) 478–488;
(h) G. Kite, N. Veitch, Rapid Commun. Mass. Spectrom. 25 (2011) 2579–2590;
(i) D. Cornett, M. Reyzer, P. Chaurand, R. Caprioli, Nat. Methods 4 (2007) 828–833;

(j) T. Sinha, S. Khatib-Shahidi, T. Yankeelov, K. Mapara, M. Ehtesham, D. Cornett, B. Dawant, R. Caprioli, J. Gore, Nat. Methods 5 (2008) 57–59;
(k) R. Cole Ed., Electrospray and MALDI Mass Spectrometry, Wiley, 2010;
(l) H. Lisa, D. Cazares, A. Dean, B. Wang, R. Richard, O. Semmes, Anal. Bioanal. Chem. 401 (2011) 17–27;
(m) A. Römpp, S. Guenther, Z. Takats, B. Spengler, Anal. Bioanal. Chem. 401 (2011) 65–73;
(n) E. Esquenazi, Y. Yang, J. Watrous, W. Gerwickac, P. Dorrestein, Nat. Prod. Rep. 26 (2009) 1521–1534.